CANCER

Bacteria-triggered tumor-specific thrombosis to enable potent photothermal immunotherapy of cancer

Xuan Yi[1], Hailin Zhou[1], Yu Chao[2], Saisai Xiong[1], Jing Zhong[1], Zhifang Chai[1], Kai Yang[1]*, Zhuang Liu[2]*

We discovered that attenuated *Salmonella* after intravenous injection would proliferate within various types of solid tumors but show rapid clearance in normal organs, without rendering notable toxicity. Bacteria-induced inflammation would trigger thrombosis in the infected tumors by destroying tumor blood vessels. Six types of tested tumors would all turn into darkened color with strong near-infrared absorbance, as observed by photoacoustic imaging. Under laser irradiation, those bacterial-infected tumors would be effectively ablated. Because of the immune-stimulation function, such bacteria-based photothermal therapy (PTT) would subsequently trigger antitumor immune responses, which could be further enhanced by immune checkpoint blockade to effectively suppress the growth of abscopal tumors. A robust immune memory effect to reject rechallenged tumors is also observed after bacteria-based PTT. Our work demonstrates that bacteria by themselves could act as a tumor-specific PTT agent to enable photoimmunotherapy cancer therapy to inhibit tumor metastasis and recurrence.

INTRODUCTION

To conquer the threat of cancer, a large variety of treatment strategies based on different mechanisms have been applied or tested in the clinic (*1*). However, conventional cancer therapies such as chemotherapy and radiotherapy have limitations in severe side effects, therapeutic resistance, and limited specificity (*2*). Light-triggered phototherapies, including photothermal therapy (PTT) and photodynamic therapy, are known to be less invasive with higher specificity but are normally applied for treatment of local tumors instead of distant metastatic ones (*3*, *4*). In 2019, Rastinehad *et al.* (*4*) reported the first clinical trial of PTT based on gold-shelled silica nanoparticles to treat patients with prostate cancer with the help of stereotactic trocar/laser fiber. Thirteen of 15 treated patients had no signs of cancer in 1 year after treatment, demonstrating the promises of laser-based PTT for clinical use (*4*). On the other side, cancer immunotherapy, by using the host's immune systems to attack tumor cells, has presented tremendous promises in recent years (*5*). For instance, immune checkpoint blockade (ICB) therapy using antibodies to block immune checkpoint receptors such as programmed cell death protein 1/programmed cell death ligand 1 (PD1/PD-L1) and cytotoxic T lymphocyte–associated protein-4 (CTLA-4) have been clinically used for treatment of various types of tumors (*6*). However, the overall clinical response rate of ICB therapy alone, which is not a tumor-specific therapy, is known to be relatively low (*7*, *8*). Therefore, the combination of ICB therapy with other types of therapeutic methods, including chemotherapy, radiotherapy, and phototherapy, has attracted a great deal of attention in recent years (*9*–*11*). For instance, the combination of PTT based on immune-adjuvant nanoparticles with ICB therapy could trigger antitumor immune responses to suppress tumor metastasis and recurrence after local tumor ablation (*11*). However, in those systems, the immune-adjuvant nanoparticles with limited tumor-homing specificity are normally locally injected into tumors to avoid side effects (e.g., cytokine storms).

Recently, live tumor-targeting microorganisms, such as bacillus Calmette-Guérin, anaerobic bacteria, and even oncolytic virus, have emerged as tumor-specific drug delivery carriers or as therapeutic agents by themselves (*12*–*15*). In particular, because of the hypoxic, immunosuppressive, and biochemically unique microenvironment within solid tumors, *Salmonella typhimurium* can selectively colonize in tumor tissues (*16*, *17*). Moreover, bacterial infection may induce innate and adaptive immune responses against both tumor-colonizing bacteria and the tumor cells, resulting in nonspecific killing of heterogeneous tumor cells (*18*, *19*). For safety reasons, *S. typhimurium* should be attenuated by different approaches to reduce their systemic toxicity (*20*–*22*). However, as shown in phase 1 clinical trials, attenuated *S. typhimurium* treatment alone usually could not effectively eliminate the tumor (*23*, *24*). To augment the antitumor efficacy of bacterial therapy, transport of therapeutic agents such as various cytotoxic agents, prodrug-converting enzymes, or immunomodulators by tumor-homing bacteria has been proposed to be an alternative strategy in cancer treatment (*25*–*27*). Recently, it has been reported that certain types of bacteria could delivery near-infrared (NIR) absorbing agents such as gold nanorods or polydopamine into tumors for photothermal tumor ablation (*28*, *29*). Nevertheless, using bacteria alone without loading of additional therapeutic agents or nanoparticles to achieve phototherapy or photoimmunotherapy has not yet been reported to our best knowledge.

In our work, a bacteria-based photoimmunotherapy is proposed using intact microbes without any chemical modification or loading of additional payloads. We accidently found that different types of solid tumors on mice with intravenous injection of low doses of the attenuated *Salmonella* ΔppGpp strain, which is defective in guanosine 5′-diphosphate-3′-diphosphate synthesis (ΔppGpp *S. typhimurium*), would show obviously darkened colors a few hours after injection. Further investigation verified that ΔppGpp *S. typhimurium* after intravenous injection could specifically colonized in the tumor, with little infection in other normal organs, owing to the facultative anaerobic habit of those bacteria and the unique hypoxic tumor microenvironment. The bacterial proliferation within tumors would trigger activation of innate immunocytes, release of proinflammatory factors,

[1]State Key Laboratory of Radiation Medicine and Protection, School of Radiation Medicine and Protection and School for Radiological and Interdisciplinary Sciences (RAD-X), Collaborative Innovation Center of Radiation Medicine of Jiangsu Higher Education Institutions, Soochow University, Suzhou, Jiangsu 215123, China. [2]Institute of Functional Nano and Soft Materials (FUNSOM), Collaborative Innovation Center of Suzhou Nano Science and Technology, Soochow University, Suzhou, Jiangsu 215123, China.
*Corresponding author. Email: kyang@suda.edu.cn (K.Y.); zliu@suda.edu.cn (Z.L.)

and disruption of the tumor vasculature, which could result in influx of blood cells into extravascular spaces within tumor where coagulation may occur. Such bacteria-induced tumor-specific thrombosis would then lead to an obviously darkened tumor color with strong NIR absorbance, as monitored by in vivo photoacoustic (PA) imaging. Because of the increased tumor-specific NIR absorbance, effective photothermal ablation of tumors could be achieved, as evidenced by five different types of tumor models (Fig. 1A). Taking advantages of the intrinsic immunostimulatory effect of bacteria, our bacteria-triggered PTT could induce potent antitumor immune responses, which, together with ICB therapy, could suppress the growth of metastatic tumors. A strong immune memory effect to prevent cancer recurrence is lastly achieved after such bacteria-triggered PTT.

RESULTS AND DISCUSSION

In vivo behaviors of attenuated *Salmonella* in mice

We first studied the behaviors of ΔppGpp *S. typhimurium* in mice after intravenous injection. ΔppGpp *S. typhimurium*, obtained from The third Xiangya Hospital of Centre South University, was made to be defective in the synthesis of ppGpp, which is a required signaling molecule to induce the expression of a number of virulence genes (*21*). In our experiments, female Bab/c mice bearing subcutaneous CT26 tumors were intravenously injected with ΔppGpp *S. typhimurium* at the dose of 5×10^6 colony-forming units (CFU) per mouse and then sacrificed at 2, 6, 12, 24, and 72 hours after injection. The major organs and tumor tissue were collected, homogenized, serially diluted (10-fold), and plated on Luria-Bertani (LB) plates. By counting the CFU in each plate, it was found that bacteria were gradually eliminated from major organs such as heart, liver, spleen, kidney, and lung. In marked contrast, the CFU in tumors increased exponentially following the time (Fig. 1, B and D). This phenomenon might be attributed to the selected colonization of anaerobes in the hypoxic, immunosuppressive, and biochemically unique tumor microenvironment (*16*, *30*).

Next, to track the long-term behaviors of ΔppGpp *S. typhimurium* in normal organs of mice, we counted live bacteria in major organs for healthy mice after intravenous injection of ΔppGpp *S. typhimurium* (5×10^6 CFU per mouse) at the appointed time points. As shown in Fig. 1 (C and E), the injected live bacteria showed accumulation mainly in the liver and spleen at early time points (e.g., days 1 and 3) and showed rapidly decreased CFU values in all examined organs. After 30 days, barely any bacterial infection was detected in mouse organs, likely due to the efficient clearance of bacteria by the immune system in normal organs (*31*, *32*).

Meanwhile, to make certain of the safety of such ΔppGpp *S. typhimurium*, hematological examinations, including complete blood panel and serum biochemistry assays, were conducted (fig. S1, A to K). On day 1 after bacteria injection, all of serum biochemistry index (fig. S1, A to C) and most of blood routine data (fig. S1, E to J) appeared to be within the normal ranges compared to untreated healthy mice, except the decrease in white blood cell (WBC) counts and platelet counts. At later time points (7 or 30 days after injection), however, both WBC counts and platelet counts for bacteria-treated mice were back into the normal ranges, suggesting that the ΔppGpp *S. typhimurium*–triggered acute inflammation, which was moderate and tolerable for mice, could be overcome within a week without chronic toxicity. Therefore, ΔppGpp *S. typhimurium* would specifically accumulate in tumor with high biosafety after injection at our tested dose.

Photothermal tumor ablation with attenuated *Salmonella*

During our experiments, there was an unexpected interesting finding that all tumors on BALB/c mice intravenously injected with bacteria showed obviously darkened color (blackish color), especially at doses above 5×10^6 CFU per mouse (Fig. 2A). PA imaging is able to record the generated ultrasonic signals from the optical absorption within tissues under pulsed light irradiation Therefore, PA imaging was used here to monitor the change of optical absorbance in those tumors on mice with bacteria injection. As shown in Fig. 2B, PA imaging of tumors under the wavelength of 750 nm revealed that the PA signals throughout the entire tumor region became much stronger after bacteria injection. The PA spectra in the tumor were also recorded (Fig. 2C). Compared to untreated tumors, tumors on mice with bacteria injection showed obviously increased PA signals from 700 to 900 nm, although the spectrum pattern was not changed. Quantitative analysis of average PA signals in the tumor regions (Fig. 2D) showed that the bacteria-induced PA signals peaked at ~12 hours after intravenous injection of ΔppGpp *S. typhimurium*. Note that the reduced PA signals inside tumors at 24 hours could be due to the rather high optical absorbance within the tumor at that time point that prevented the light penetration during imaging.

The darkened tumor color and enhanced PA signals in the tumor in the wavelength range of 700 to 900 nm suggested that tumors on bacteria-injected mice would show increased NIR absorbance, which could be used for photothermal heating under NIR laser. Therefore, at 12 hours after injection of bacteria at different doses, the tumors of those mice were irradiated by an 808-nm laser at the power density of 0.8 W/cm^2 for 8 min. As recorded by an IR camera, the tumor temperature on bacteria-injected mice showed rapid increase under laser irradiation, which at the current power density would not induce significant heating to control mice injected with phosphate-buffered saline (PBS) (Fig. 2E). It was found that the tumor-surface temperature increased to 45.5°, 54.9°, and 63.1°C under 808-nm laser irradiation for mice injected with bacteria at 5×10^5, 5×10^6, and 5×10^7 CFU per mouse, respectively (fig. S2).

The average tumor sizes and body weights were then monitored for mice after various treatments, including (i) PBS, (ii) 808-nm laser irradiation, (iii) bacteria injection at 5×10^5 CFU per mouse, (iv) bacteria injection at 5×10^6 CFU per mouse, (v) bacteria injection at 5×10^7 CFU per mouse, (vi) bacteria injection at 5×10^5 CFU per mouse plus laser, and (vii) bacteria injection at 5×10^6 CFU per mouse plus laser (Fig. 2, F and G). At a high dose of ΔppGpp *S. typhimurium* (5×10^7 CFU per mouse), although the tumor growth showed significant delay even without laser irradiation, the mouse body weights showed a rapid drop, and two of five mice died in this group (Fig. 2G), suggesting the severe toxicity of bacteria at such a high dose. Under reduced doses at 5×10^5 and 5×10^6 CFU per mouse, the mouse body weight drop appeared to be much less significant, and no animal death was observed after injection. Meanwhile, although bacteria treatment alone at reduced doses (5×10^5 and 5×10^6 CFU per mouse) could not inhibit the tumor growth, laser irradiation of tumors on mice injected with 5×10^6 CFU per mouse could result in complete ablation of those tumors (Fig. 2F). Therefore, ΔppGpp *S. typhimurium* at a moderate dose (5×10^6 CFU per mouse) could be used for effective photothermal tumor ablation with a tolerable side effect.

The next question is why the bacteria injection would change the optical absorbance of tumors. Considering the unchanged PA spectra of tumor before and after bacteria injection (Fig. 2C), we suspected that the increased NIR absorbance in the tumor could be contributed

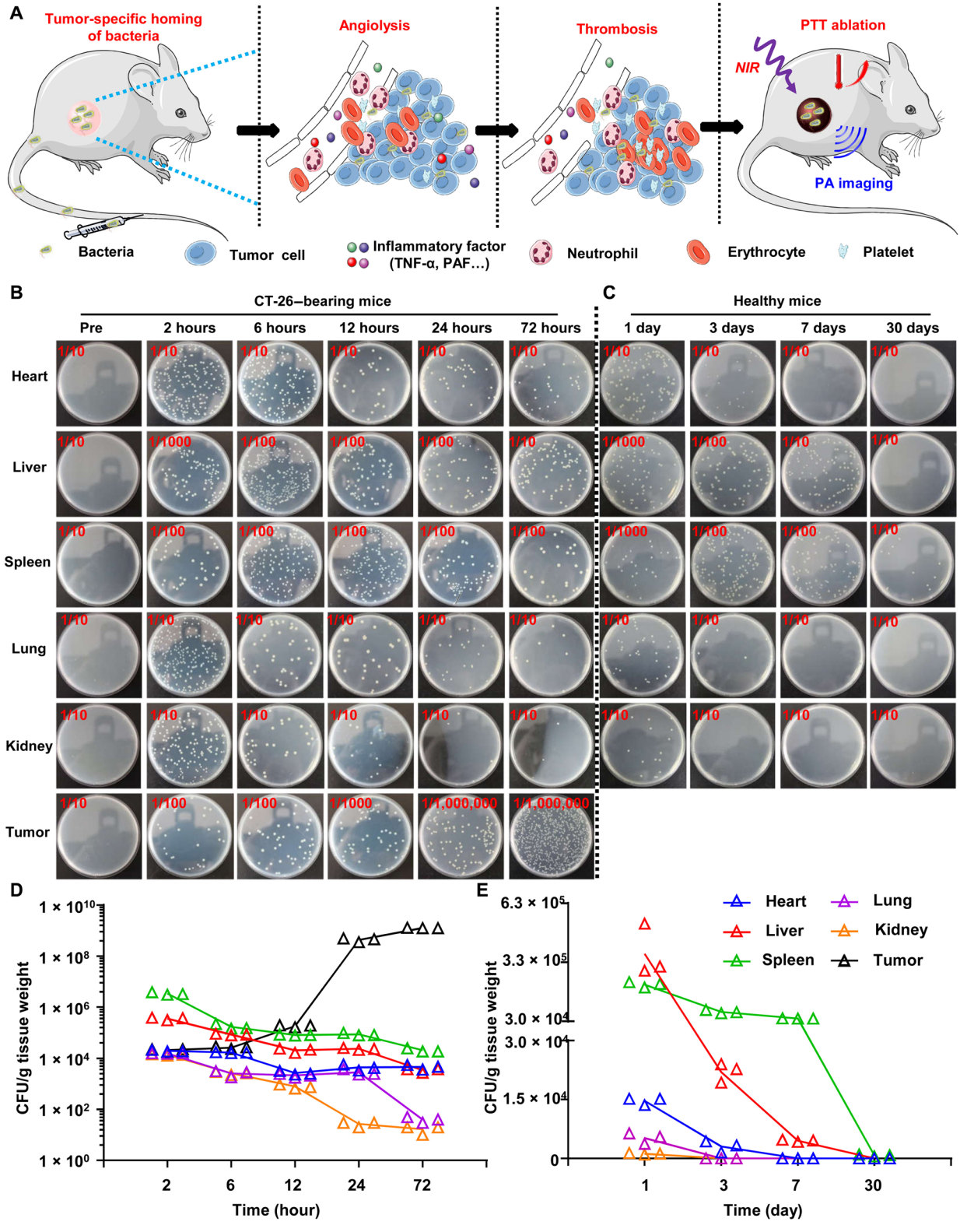

Fig. 1. Bacterial colonization in CT26-bearing mice and healthy mice after intravenous injection. (**A**) Schematic illustration of bacteria-triggered tumor thrombosis and the subsequent photothermal tumor ablation. The enhanced NIR absorbance of the tumor is visualized by in vivo PA imaging. (**B** and **D**) Representative photographs of solid Luria-Bertani (LB) agar plates (B) and quantification (D) of bacterial colonization in various organs harvested from CT26-bearing mice at different time points after injection of bacteria. (**C** and **E**) Representative photographs of solid LB agar plates (C) and quantification (E) of bacterial colonization in various organs of healthy mice in a month. Photo credit: Xuan Yi, Soochow University.

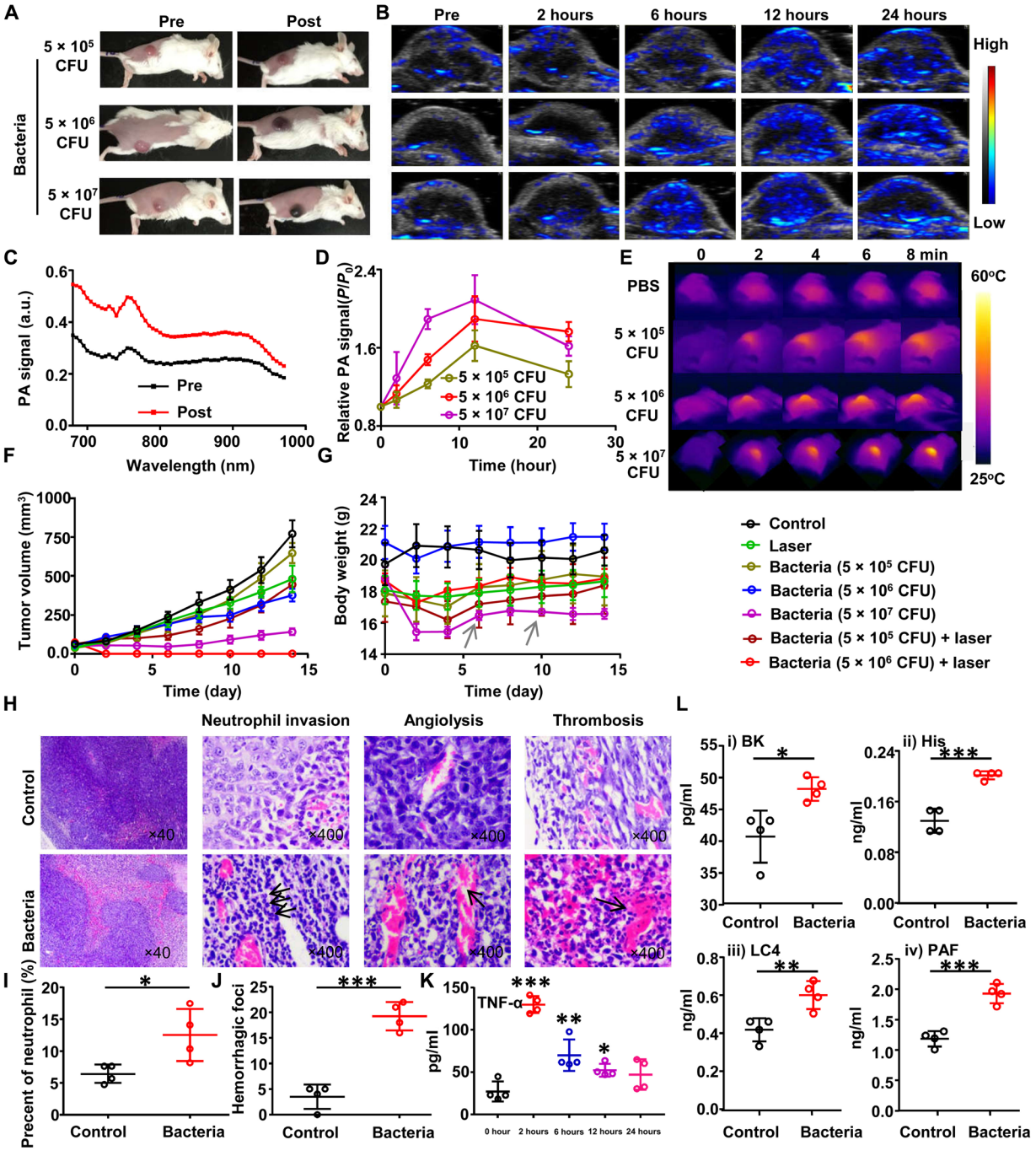

Fig. 2. Bacteria-triggered photothermal ablation of CT26 tumors. (**A**) Photographs of BALB/c mice before or after injection of bacteria at the doses of 5×10^5 colony-forming units (CFU), 5×10^6 CFU, and 5×10^7 CFU. (**B**) Representative PA images tumors on mice intravenously injected with different doses of bacteria. (**C**) PA spectra from 680 to 980 nm for CT26 tumors on mice before or after injection of bacteria. (**D**) Quantification of relative PA signals of CT26 tumors on mice injected with bacteria at the doses of 5×10^5 CFU, 5×10^6 CFU, and 5×10^7 CFU. Data are presented as the mean ± SD. (**E**) Representative IR thermal images of the mice injected with bacteria at the doses of 5×10^5 CFU, 5×10^6 CFU, and 5×10^7 CFU under 808-nm laser irradiation. (**F**) Tumor growth curves of mice with different treatments indicated ($n = 5$ per group). Data are presented as the mean ± SEM. (**G**) Average body weights of mice after various treatments indicated. The gray arrow represents the death of mouse. Data are presented as the mean ± SEM. (**H**) Representative images of hematoxylin and eosin (H&E)–stained tumor slices collected from mice injected with phosphate-buffered saline (PBS) or bacteria. (**I** and **J**) Quantification to show percentages of neutrophils (I) and hemorrhagic foci (J) based on H&E-stained images. (**K**) The tumor necrosis factor–α (TNF-α) levels in sera from mice isolated at 0, 2, 6, 12, and 24 hours after bacteria injection. *P* values were determined between TNF-α level at 0 hour and that at other time points. (**L**) The inflammatory factors including bradykinin (BK), histamine (His), leukotriene C4 (LC4), and platelet-activating factor (PAF) levels in sera from mice isolated before or 12 hours after bacteria injection. Data are presented as the mean ± SD. Statistical analysis was performed using the Student's two-tailed *t* test (***$P < 0.001$, **$P < 0.01$, and *$P < 0.05$). a.u., arbitrary unit. Photo credit for (A): Xuan Yi, Soochow University.

to the formation of blood coagulation within the tumor. As shown in fig. S3A, the blood sample had a wide absorbance from 600 to 1000 nm due to the optical absorbance of hemoglobin. Under the 808-nm laser irradiation, the photothermal heating effect for diluted blood samples showed positive correlation with the concentrations of blood. Moreover, the optical absorbance and photothermal performance could be further enhanced when the blood was coagulated because of the higher concentration of hemoglobin in blood clots (fig. S3, B and C). Therefore, it is speculated that the enhanced optical absorbance in tumors of mice after bacteria injection might be attributed to the local thrombosis that leads to concentrated blood coagulates within the tumor.

To confirm the above hypothesis, we collected CT26 tumors on mice injected with bacteria at the dose of 5×10^6 CFU per mouse for hematoxylin and eosin (H&E) staining (Fig. 2, H to J). In a large view, we could find severe hemorrhagic inflammation in tumors on mice injected with bacteria. Compared with normal tumor tissue, neutrophil invasion, a representative feature in bacterial infection, could be abundantly found in the tumor after bacterial infection (Fig. 2, H and I). In particular, significant angiolysis and obvious thrombosis could be observed in tumor slices from bacteria-injected mice (Fig. 2, H and J). Moreover, the tumor vascular destruction after bacteria injection was also observed by immunofluorescent staining of CD31, a marker of blood vascular endothelial cells (fig. S4). We directly tested the hemoglobin content in tumors collected from the mice injected with bacteria at different time points. We could find that the hemoglobin content in tumor sites was increased obviously after injection of bacteria (fig. S5). Therefore, colonization of ΔppGpp *S. typhimurium* within the tumor could trigger tumor-specific thrombosis by disrupting tumor blood vessels.

Next, we checked the release of tumor necrosis factor–α (TNF-α), a cytokine that could induce influx of blood into the tumors by vascular disruption (*17*), and a number of proinflammatory factors in sera of treated mice. We did observe obviously increased TNF-α in mouse serum at 2 hours after injection of bacteria. The measured serum levels of TNF-α showed gradual decrease overtime and returned back to the normal level after 24 hours (Fig. 2K). Besides, the concentrations of the vasodilator inflammatory factor, including bradykinin (BK), histamine (His), leukotriene C4 (LC4), and platelet-activating factor (PAF), which could enhance the vascular permeability, showed significant elevation (Fig. 2L). All of the above cytokines could enlarge the vascular void, resulting in the blood influx and thrombosis with the help of platelet activation in extravascular area (*33*).

Notably, the angiolysis triggered by bacteria appeared to be specific to the tumor but not to other normal organs (fig. S6). The tumor blood vessels with relatively low rates of flow and high permeability may be particularly sensitive to the effects of antivascular agents (*34*). Meanwhile, the tumor-specific colonization of anaerobic bacteria would be another reason for such tumor-specific angiolysis and thrombosis triggered by ΔppGpp *S. typhimurium*.

Thereafter, we checked another strain of *Salmonella* (VNP20009), *Escherichia coli K88*, and *Lactobacillus kimchii* to examine whether this phenomenon was unique to the ΔppGpp *S. typhimurium* strain. From the photographs of CT26 tumor–bearing mice injected with the abovementioned bacteria, we found that Gram-negative bacteria, including *Salmonella* VNP20009 and *E. coli* K88, could induce darkened color for the tumors, while Gram-positive bacteria *L. kimchii* could not. Considering that lipopolysaccharides (LPS) are a major component of the cell walls of Gram-negative bacteria, we directly injected LPS (from *Salmonella typhosa*) at different doses into the mice. From the photos of mice injected with LPS, the darkened tumor tissues could be induced by LPS alone (fig. S7). Therefore, we speculated that LPS existing in the cell wall of Gram-negative bacteria might play an important role in triggering tumor-specific thrombosis, although the detailed mechanisms remain to be further investigated in future studies.

Next, we wondered whether such phenomenon would be a general behavior for different types of tumors. BALB/c mice bearing four different types of tumor models, including mouse breast cancer 4T1 tumors, human malignant glioblastoma U87MG tumors, human pancreatic cancer SW1990 tumors, human lung cancer A549 tumors, or patient-derived cervical cancer (patient-derived xenografts, PDX), were intravenously injected with ΔppGpp *S. typhimurium* at the dose of 5×10^6 CFU per mouse. Similar to high accumulation of bacteria in CT26 tumors, bacteria would colonize in aforementioned tumor models at 24 hours after injection (fig. S8A). As easily observed by naked eyes, all tumors on mice with bacteria injection turned into black color in a few hours (Fig. 3A and fig. S9A). In vivo PA imaging was further carried out to image those tumors (Fig. 3B and fig. S9A). Similar to that observed for CT26 tumors, strong PA signals also showed up in those tumors after mice were injected with bacteria, and the peaked PA intensities were observed between 6 and 12 hours after injection. (Fig. 3C and fig. S9B). Photothermal heating of those tumors was further conducted by using the 808-nm laser at the power density of 0.8 W/cm^2 to irradiate those tumors, which all showed rapid laser-induced temperature increase (Fig. 3D and fig. S8, B and C). Moreover, as revealed by the tumor growth curves (Fig. 3, E to H, and fig. S9C), complete tumor destruction with a tolerable toxicity (figs. S9D and S10) was achieved by such bacteria-triggered PTT for all four types of tumor models, similar to that observed with CT26 tumors. In addition, the injection of ΔppGpp *S. typhimurium* into the C57BL/6 mice bearing MC-38 tumor could also induce color darkening of the tumors at an increased bacteria dose (fig. S11). Therefore, our experiments demonstrated that tumor darkening and PTT induced by tumor-homing bacteria could be applicable for various types of solid tumors on different mouse strains.

Bacteria-induced photoimmunotherapy

It has been reported that certain types of bacterial infection in solid tumors could establish a more immunogenic microenvironment, such as activating dendritic cells (DCs) or sensitizing the tumors to ICB therapy (*35*–*37*). Moreover, flagellin, a subunit protein of the bacterial flagellum, could improve $CD8^+$ T cell–dependent antitumor responses and decrease the frequency of $CD4^+CD25^+$ regulatory T (T_{reg}) cells (*38*, *39*). Therefore, we studied the immunological responses after tumors on mice were ablated by bacteria-triggered PTT. Antigen-presenting cells (APCs) such as DCs are able to capture and process antigens to activate T cells and trigger subsequent immune responses. The maturation of DCs is a critical initial step in this process. At the in vitro level, we incubated DCs isolated from the bone marrow of 8-week-old BALB/c mice with different concentrations of heat-treated bacteria (obtained after 15 min of 90°C heat treatment) for 12 hours. Markedly enhanced maturation of DCs was observed after they were treated with debris of bacteria (fig. S12, A and B), indicating that bacteria after PTT ablation may act as an immune stimulatory agent similar to the function of immune adjuvants.

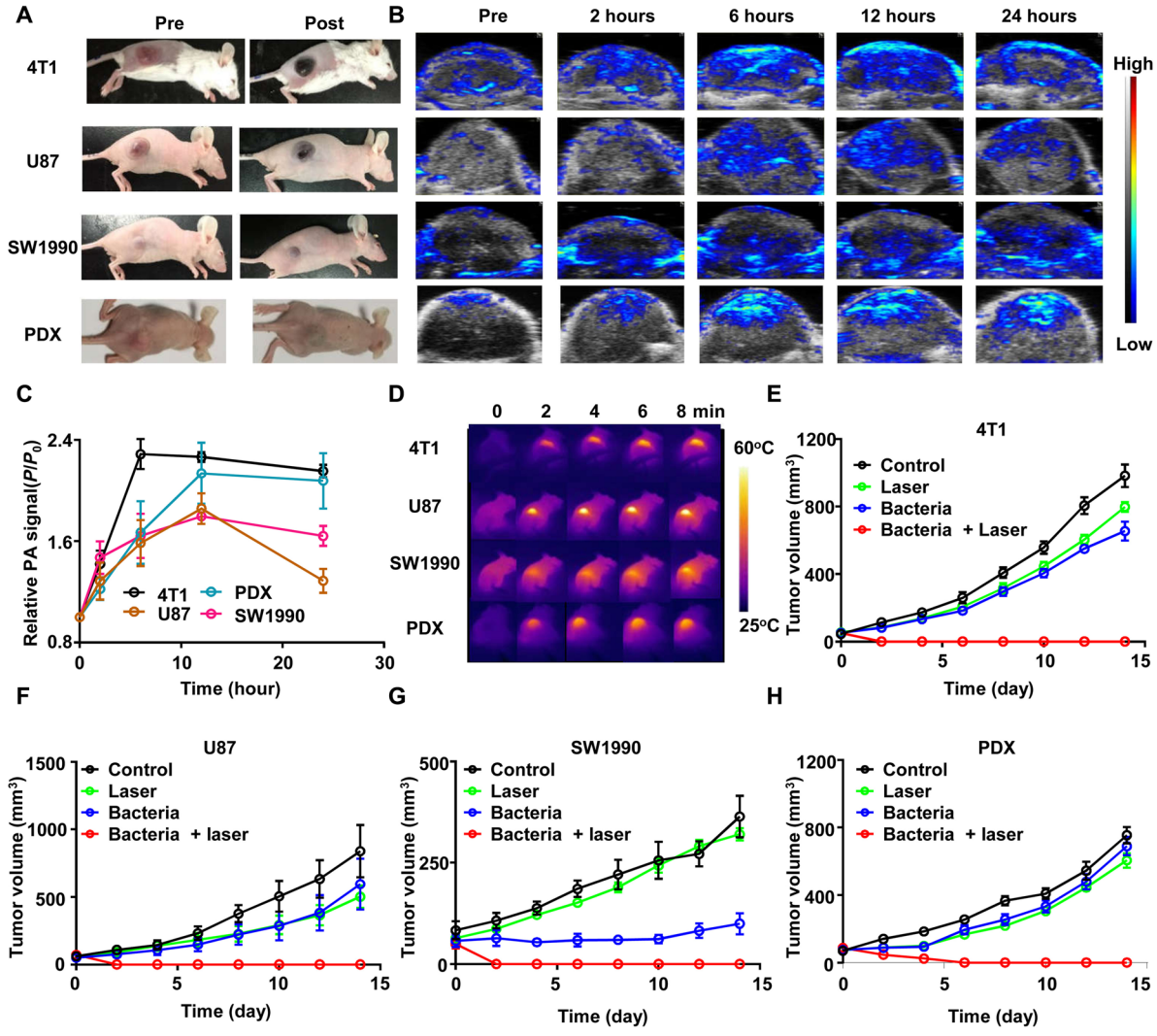

Fig. 3. Bacteria-triggered photothermal ablation of other tumor models. (**A**) Photographs of BALB/c mice bearing 4T1, U87MG, SW1990, and patient-derived xenografts (PDX) tumors, before and after injection of bacteria at the dose of 5×10^6 CFU. (**B**) Representative PA images of different types of tumors on mice injected with bacteria at the dose of 5×10^6 CFU. (**C**) Quantification of relative PA signals of tumors on mice injected with 5×10^6 CFU of bacteria. Data are presented as the mean ± SD. (**D**) Representative IR thermal images of the tumor-bearing mice injected with bacteria at the dose of 5×10^6 CFU under 808-nm laser irradiation. (**E** to **H**) Tumor growth curves of mice bearing different kinds of tumor models, including 4T1 tumors (E), U87MG tumors (F), SW1990 tumors, (G) and PDX tumors (H), with different treatments indicated. Five mice were used for each group. Data are presented as the mean ± SEM. Photo credit for (A): Xuan Yi, Soochow University.

Next, the in vivo DCs maturation triggered by bacteria-based PTT was evaluated. To distinguish the antitumor immune stimulation effect induced by bacteria-triggered photothermal or pure photothermal treatment, we selected the polyethylene glycol (PEG)–grafted poly(lactic-*co*-glycolic) acid (PLGA) with indocyanine green (ICG) loading (PLGA-PEG-ICG) as a common photothermal reagent. ICG as the NIR dye is a U.S. FDA (Food and Drug Administration)–approved agent. CT26 tumors grown on BALB/c mice were removed by different treatments including (a) surgery, (b) PLGA-PEG-ICG plus surgery, (c) PLGA-PEG-ICG plus laser, (d) bacteria plus surgery, and (e) bacteria plus laser. As the control, PLGA-PEG-ICG nanoparticles were intravenously injected into CT26 tumor–bearing mice (10 mg/kg ICG per mouse) (*18*). On the basis of our previous study, PLGA-PEG-ICG nanoparticle showed the highest tumor accumulation at 24 hours after injection. (*11*). Therefore, after 24 hours, tumors on mice were irradiated under 808-nm laser for 8 min (0.8 W/cm^2). The ipsilateral inguinal lymph nodes nearby those tumors were harvested 2 days later and homogenized into single-cell suspensions, which were then stained with fluorescently labeled anti-CD11c, anti-CD86, and anti-CD80 antibodies for flow cytometry assay (Fig. 4, A and B). Compared to the surgery group (group a), bacteria injection after surgery (group b) could stimulate DC maturation in the lymph nodes. On the other hand, while PLGA-PEG-ICG nanoparticles (group b) showed no immune stimulation effect, PTT with PLGA-PEG-ICG (group d) could also trigger DC maturation to a moderate level. This could be attributed to the release of tumor-related antigens after PTT (*11*). Notably, the highest level of DC maturation was observed for the bacteria-triggered PTT group (group e). Therefore, the tumor debris after PTT (as tumor-associated antigens) and bacteria (as an adjuvant) could function together to elicit

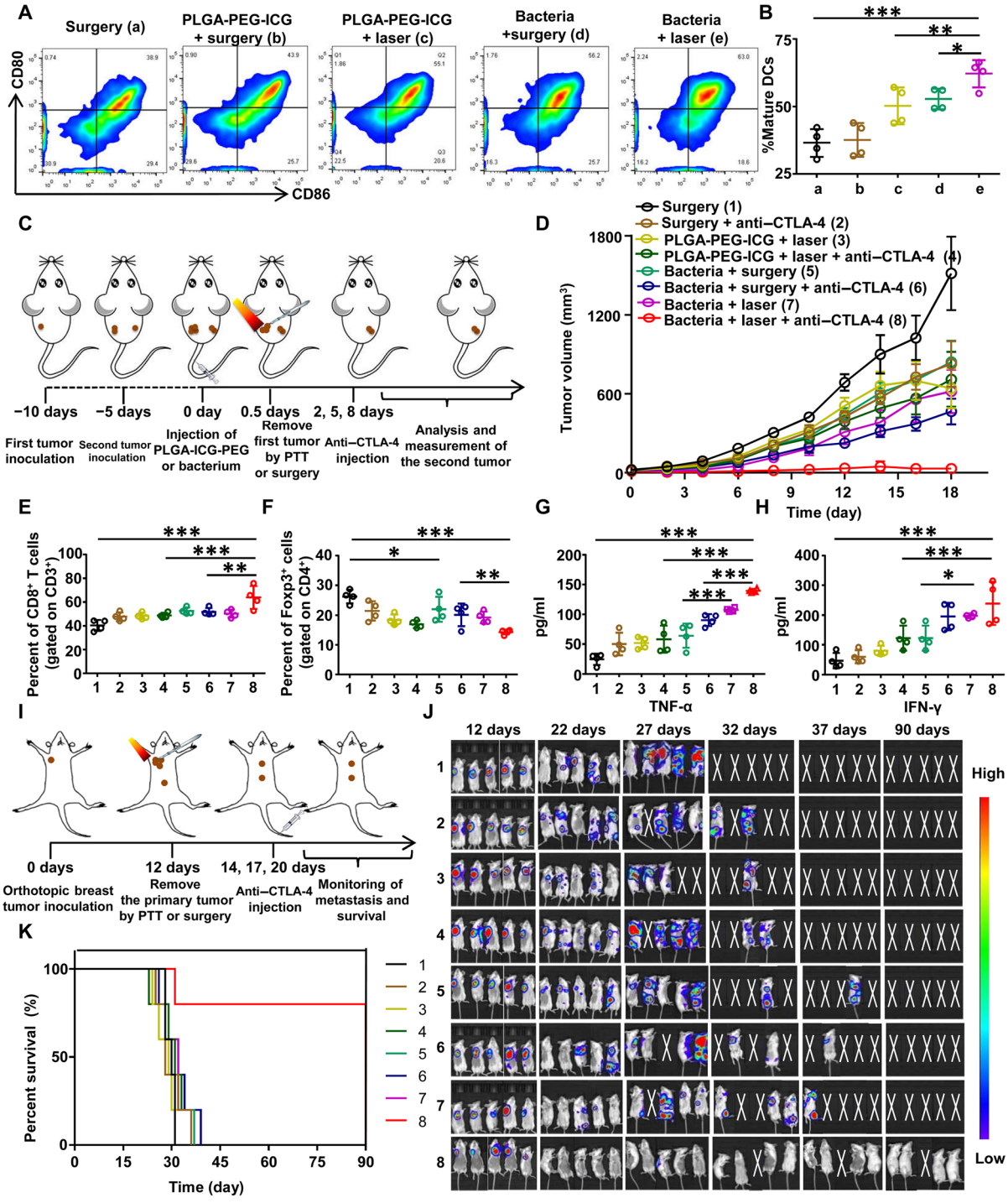

Fig. 4. Bacteria-induced photothermal immunotherapy. (**A** and **B**) Representative flow cytometry plots (A) and quantification (B) of DC maturation induced by bacteria-based PTT on mice bearing CT26 tumors (gated on $CD11c^+$DC cells). Cells in the tumor-draining lymph nodes were collected 72 hours after various treatments for flow cytometry assessment after staining of CD11c, CD80, and CD86. Data are presented as the mean ± SD. (**C**) Schematic illustration of bacteria-based photothermal immunotherapy to inhibit tumor growth at distant sites. (**D**) The growth curves of secondary abscopal tumors for different groups of mice (five mice per group) with after various treatments to eliminate their primary tumors. Data are presented as the mean ± SEM. (**E** and **F**) Proportions of tumor-infiltrating $CD8^+$ killer T cells among $CD3^+$ cells (E) and proportions of $CD4^+FoxP3^+$ regulatory T cells among $CD4^+$ cells (F) in the abscopal CT26 tumors at day 10. (**G** and **H**) The TNF-α level (G) and interferon-γ (IFN-γ) level (H) in sera from mice isolated at day 10. (**I**) Schematic illustration of bacteria-based photothermal immunotherapy to inhibit spontaneous metastases. (**J**) In vivo bioluminescence images to track the spreading of fLuc-4T1 cancer cells in different groups of mice after various treatments to eliminate their primary breast tumors. (**K**) Morbidity-free survival of different groups of mice-bearing orthotopic 4T1 tumors with spontaneous metastases after various treatments indicated to eliminate their primary breast tumors (10 mice per group). Data are presented as the mean ± SD. Statistical analysis was performed using one-way analysis of variance (ANOVA) with the least significant difference post hoc test (***$P < 0.001$, **$P < 0.01$, and *$P < 0.05$).

immune responses, which may be tumor specific and would be helpful to offer an abscopal therapeutic effect to attack distant tumors that cannot be reached by laser irradiation.

To further enhance the antitumor immunity after bacteria-based PTT, the antibody against CTLA-4 (anti–CTLA-4), which has been approved by the FDA to inhibit the activities of immune-suppressive T_{regs}, was introduced in our work. In the first animal model, two CT26 colorectal tumors were inoculated on two flanks of each mouse in succession. The primary tumor was eliminated by four different treatments, including surgery (groups 1 and 2), PLGA-PEG-ICG plus laser (groups 3 and 4), bacteria plus surgery (groups 5 and 6), and bacteria plus laser (groups 7 and 8). After removal of primary tumors, mice in groups 2, 4, 6, and 8 were injected with the anti–CTLA-4 at the days 2, 5, and 8 at the dose of 20 μg per mouse for each time. The sizes of distant tumors were monitored afterward (Fig. 4C). Compared to mice with surgery removal of their primary

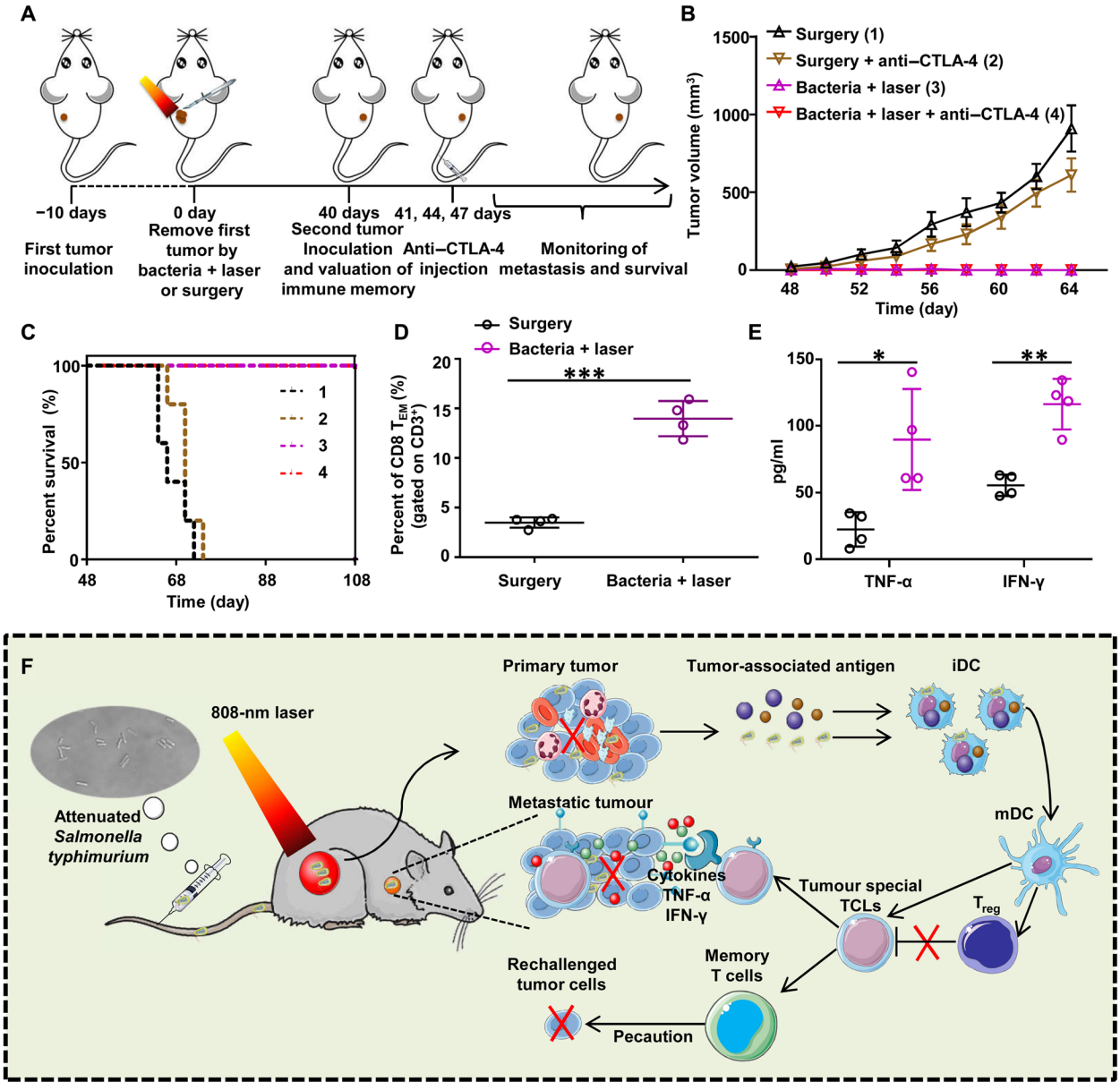

Fig. 5. Long-term immune-memory effects. (**A**) Schematic illustration of bacteria-based PTT therapy to inhibit cancer relapse. (**B**) Tumor growth curves of rechallenged tumors inoculated 40 days after elimination of their first tumors (eight mice per group). Data are presented as the mean ± SEM. (**C**) Morbidity-free survival of different groups of mice with rechallenged CT26 tumors after various treatments indicated to eliminate their primary tumors (10 mice per group). Bacteria-based PTT, even in the absence of anti–CTLA-4 blockade, could trigger strong enough immune responses to reject rechallenged tumor. (**D**) Quantification of proportions of $CD8^+$ effector memory T cells (T_{EM}) gated on $CD3^+$ cells in the spleen analyzed at day 40 right before rechallenging mice with secondary tumors. (**E**) Cytokine levels, including TNF-α and IFN-γ, in sera from mice isolated at day 47. Data are presented as the mean ± SD. Statistical analysis was performed using the Student's two-tailed *t* test (***$P < 0.001$, **$P < 0.01$, and *$P < 0.05$). (**F**) Schematic illustration of bacteria-based photothermal immunotherapy to inhibit the growth of primary tumors, abscopal metastatic tumors, and rechallenged tumors.

tumors, substantial abscopal effects in inhibiting the growth of distant tumors were observed for mice with their primary tumors eliminated by PTT, especially by bacteria-based PTT. The most impressive abscopal effect was observed for the combination of bacteria-triggered PTT with anti–CTLA-4 therapy, which resulted in nearly complete suppression of distant tumors after their primary tumors were ablated by PTT. Notably, the combination of PLGA-PEG-ICG–based PTT with anti–CTLA-4 appeared to be less effective in inhibiting the distant tumors, likely due to the lack of immune stimulation effect of such PLGA-based nanoparticles (Fig. 4D and figs. S13 and S14). Therefore, the adjuvant-like immune stimulation effect of bacteria after PTT ablation of primary tumors is critical to achieve the abscopal antitumor immune responses in such photothermal immunotherapy.

To analyze the immune mechanism of distant tumor inhibition, the components of immune cells and content of immune cell cytokines, including TNF-α and interferon-γ (IFN-γ), were tested in our work (Fig. 4, E to H). It was found that the percentage of $CD3^+CD8^+$ T cells (Fig. 4E and fig. S15A), which represent CTLs, showed the most significant increase in group 8, which was treated by the combination of bacteria-based PTT with anti–CTLA-4. Meanwhile, as expected, anti–CTLA-4 treatment could effectively suppress the percentages of $CD3^+CD4^+FoxP3^+$ immunosuppressive T_{reg} cells (Fig. 4F and fig. S15B). The CTL/T_{reg} ratio, a critical indicator of antitumor immune balance, was observed to be the highest in group 8 with the combined bacteria-based PTT and anti–CTLA-4 therapy, consistent to the tumor growth data. Moreover, we also found that the serum levels of TNF-α and IFN-γ, which, as the representative cytokines of cellular immunity play important roles in tumor immunotherapy, were found to be the highest in group 8 (Fig. 4, G and H). Therefore, bacteria-triggered PTT could effectively activate the cell immunity to inhibit distant abscopal tumors with the help of anti–CTLA-4.

Besides the subcutaneous tumor model, an orthotopic breast cancer model, which could undergo spontaneous metastasis, was also tested in this work to verify the ability of bacteria-based photothermal immunotherapy in metastasis inhibition after photothermal ablation of primary tumors. This tumor model was established by injecting the murine breast cancer 4T1 cells with firefly luciferase expression 4T1 (fLuc-4T1) into the breast pad of mouse (Fig. 4I). The primary breast cancer tumors of mice in each group were treated by either surgery or bacteria-based PTT on day 10, when the spontaneous metastases should have already occurred (*11*). Afterward, anti–CTLA-4 at dose of 20 μg per mouse for each injection was intravenously injected at days 14, 17, and 20. Thereafter, the metastases of tumor cells in the eight groups of mice following the same group order for the subcutaneous tumor model experiment (Fig. 4D) were recorded by in vivo bioluminescence imaging (Fig. 4J). It was also found that mice in the group 8 with bacteria-based PTT plus anti–CTLA-4 treatment showed the most effective inhibition of tumor metastasis, in marked contrast to other groups of mice in which spontaneous metastases showed up soon or later even their primary tumors were removed (Fig. 4J). While all of the mice in groups (1 to 7) died within 45 days, bacteria-based PTT plus anti–CTLA-4 (group 8) resulted in 80% of animal survival in 90 days (Fig. 4K). Therefore, bacteria-based photothermal immunotherapy could inhibit tumor metastasis and prolong the survival of mice after ablation of their primary tumors.

It is expected that powerful immunity activation may immune memory effect to prevent the same disease from happening again over a long period of time. Therefore, we wondered whether immune memory could be induced by the bacteria-based PTT of primary tumor. The experiment design is shown in Fig. 5A. At 40 days after removal of the first CT26 tumor by either surgery (groups 1 and 2) or bacteria-based PTT (groups 3 and 4), a secondary CT26 tumor was inoculated onto each mouse. Mice in group 2 and group 4 were intravenously injected with anti–CTLA-4 antibody at days 41, 44, and 47 (20 μg per mouse for each dose). The growth of their secondary tumors and body weights were then monitored (Fig. 5B and fig. S16). For mice with surgical removal of their first tumors, their second tumors rechallenged 40 days later showed rapid growth, even with the treatment of anti–CTLA-4. For mice with bacteria-based PTT to eliminate their first tumors, no appreciable growth of their rechallenged second tumors was observed, regardless of anti–CTLA-4 treatment. As the results, all mice in groups 3 and 4 survived posttumor rechallenge for over 108 days (Fig. 5C). Therefore, bacteria-based PTT resulted in a robust immune memory effect to protect mice from rechallenged tumors, and anti–CTLA-4 treatment appeared to be not essential for the immune-memory effect.

To explain the mechanism of such powerful immune memory induced by bacteria-based PTT, memory T cells and related cytokines, including TNF-α and IFN-γ, were analyzed by flow cytometry or tested by enzyme-linked immunosorbent assay (ELISA). Both central memory T cells (T_{CM}) and effector memory T cells (T_{EM}) were collected from the spleen of CT26 tumor–bearing mice at day 40 after removing their tumor by surgery or bacteria-based PTT. It is known that T_{EM} cells that can elicit immediate immune protections by producing cytokines are primarily responsible for the immune memory effect (*40*). From the flow cytometry data, it was found that the percentage of T_{EM} cells ($CD3^+CD8^+CD62L^-CD44^+$) showed significant increase for mice with primary tumors removed by bacteria-based PTT (Fig. 5D). In addition, compared with the mice with primary tumor removed by surgery, the mice with primary tumors eliminated by bacteria-based PTT showed significantly increased serum levels of TNF-α and IFN-γ on day 47, indicating that the strong antitumor immune responses had been triggered after rechallenging mice with CT26 cells (Fig. 5E).

In this work, we found that attenuated *S. typhimurium* after intravenous injection would accumulate specifically in the tumor and then trigger tumor thrombosis due to the release of TNF-α and the proinflammatory factors. After the formation of blood clots within the tumor, the tumor color would turn into black with greatly increased absorbance in the NIR region, as monitored by in vivo PA imaging. Notably, such bacteria-induced thrombosis is specific to the tumor and occurs for various tumor models, but would not happen in normal organs. Thereafter, we further found that NIR laser irradiation of those tumors on bacteria-injected mice could result in significant photothermal heating for tumor ablation, as evidenced by five different types of tumor models. In addition to the function to enable tumor PTT, such tumor-homing bacteria could act as immune-stimulatory agents to boost systemic antitumor immune responses triggered by tumor-associated antigens generated after PTT tumor ablation. With the help of anti–CTLA-4 checkpoint blockade therapy, the growth of distant tumors and spontaneous tumor metastases could be effectively suppressed after bacteria-based PTT, which in the meanwhile would offer a long-term immune memory effect to protect mice from rechallenged tumors. This whole process is described in Fig. 5F.

This work is the first demonstration of using unmodified bacteria without loading of artificial components to trigger photothermal tumor ablation and photothermal immunotherapy of cancer. Because

of the unique anaerobic feature, such attenuated *S. typhimurium* shows inherent tumor-specific colonization ability with little retention in normal organs and insignificant toxicity to treated animals. Compared to artificial nanoparticles used for photothermal and photothermal immunotherapy, such bacteria-based approach exhibits superior tumor selectivity. Therefore, attenuated *S. typhimurium* with reduced toxicity, tumor-specific homing after systemic administration, and the ability to trigger tumor thrombosis and enable photothermal tumor ablation under NIR laser and the function in immune stimulation would be a promising class of bio-agent in combinational cancer therapy. Notably, such bacteria-based therapeutic method may easily be translated into clinical trials as attenuated *S. typhimurium* has already been tested in the clinic.

MATERIALS AND METHODS

Bacteria culture

ΔppGpp *S. typhimurium* prepared by the reported method (*25*) was obtained from the Third Xiangya Hospital of Central South University and stored at −80°C. For bacterial culture, attenuated *S. typhimurium* was streaked on the bacteria LB solid plate and then incubated at 37°C for overnight. Bacteria colonies were picked out and grown overnight in LB liquid medium in a shaking incubator (37°C, 220 rpm). Afterward, the bacteria-containing medium was diluted by 50-folds into fresh medium and further grown to the early stationary phase. Thereafter, the bacteria were collected by centrifugation (5000 rpm, 16°C, 10 min) and diluted with sterile PBS for further experiments.

Tumor models

Female BALB/c mice (6 to 8 weeks) and female nude mice were purchased from Nanjing Pengsheng Biological Technology Co. Ltd. and used under protocols approved by the Institutional Animal Care and Use Committee of Soochow University. To generate the mouse tumor models, CT26 (1×10^6) and 4T1 (1×10^6) cells were subcutaneously implanted into normal BALB/c mice, while A549 (2×10^6), SW1990 (2×10^6), and U87MG (2×10^6) cells were subcutaneously implanted into nude mice. For the PDX tumor model, first, we collected the patient' cervical cancer tissue from patient in The First Affiliated Hospital of Soochow University with the patient's informed consent. Then, we put the fresh cancer tissue (after surgical resection) into growth medium and cut it into pieces (~2 to 4 mm) in a sterile dish. Last, we implanted the tumor pieces into the back of each female nude mouse under general anesthesia and then closed the skin incision. All above experiments were conducted following the relevant ethical regulations.

Bacterial colonization in vivo

We collected the major organs of mice with bacteria injection at desired time points. The major organs, including heart, liver, spleen, lung, kidney, and tumor, were extracted, weighed, and homogenized at 4°C in sterile PBS (pH = 7.2). Those samples were diluted (10-fold) and plated on LB plates. After 6 hours of incubation, bacterial colonies were counted. The bacterial titer (CFU per gram of tissue) was calculated with colony counts and tissue weights.

In vivo toxicity study

Three groups (five mice per group) of healthy mice treated with ΔppGpp *S. typhimurium* at the dose of 5×10^6 CFU per mouse were sacrificed at 1, 7, and 30 days after injection, respectively. Five healthy mice without any treatment were used as controls. Blood samples (~0.8 ml for each mouse) were collected for blood biochemistry analysis.

Thrombus analysis

The tumor tissues were collected from CT26-bearing mice intravenously injected with bacteria (1×10^6 CFU per mice) for H&E staining. The tumor blood vessels were recognized by immunofluorescent staining using CD31 antibody and Cy3-conjugated second antibody. To directly test the hemoglobin content in tumors, the collected tumors from the mice injected with bacteria were weighted and homogenized in 1 ml of ice-cold sterile PBS. ACK lysing buffer was then added and then incubated for 10 min at room temperature to allow the lysis of erythrocytes. Afterward, the samples were centrifuged (13,000 rpm, 10 min), and the optical density at 540 nm of the supernatants was recorded.

PA imaging

At different time points (0, 2, 6, 12, and 24 hours), the tumors of mice intravenously injected with bacteria were imaged by a small-animal PA imaging system (VisualSonics). The central zones of the tumor were selected as region of interest to calculate the average tumor PA signals.

Photothermal therapy

For tumor-bearing mice, at 12 hours after intravenous injection of bacteria, or at 24 hours after intravenous injection of PLGA-PEG-ICG, an 808-nm NIR laser (Changchun New Industries Optoelectronics Technology Co. Ltd.) was used to irradiate their tumors at the power density of 0.8 W/cm^2 for 8 min. The tumor temperatures were recorded by an IR camera (FLIR E50).

DC mature in vitro and in vivo

DCs were isolated from the bone marrow of 8-week-old BALB/c mice according to a published method (*11*). To perform in vitro DCs stimulation experiments, DCs were incubated with different concentrations of heat-treated bacteria for 12 hours. Afterward, DCs were collected and stained with anti–CD11c–fluorescein isothiocyanate (FITC; Invitrogen, clone: N418, lot: 2028656), anti–CD86-PE (Phycoerythrin) (Invitrogen, clone: GL1, lot: 4346386), and anti–CD80-APC (Invitrogen, clone: 16-10A1, lot: 4329685), and then classified by flow cytometry (BD FACSCalibur). For in vivo DC stimulation experiments, DCs were harvested from the ipsilateral inguinal lymph nodes of tumor-bearing mice 2 days after different treatments to eliminate their tumors, including surgery, PLGA-PEG-IC plus surgery, PLGA-PEG-ICG plus laser, bacteria plus surgery, and bacteria plus laser. Then, the DCs were stained with antibodies for flow cytometry assay.

Distant tumor inhibition

Mice were randomly divided to eight groups. For the first tumor inoculation, CT26 cells (1×10^6) were subcutaneously injected into the left flank of each mouse. For the second tumor inoculation, which was conducted 5 days later, CT26 cells (4×10^5) were subcutaneously injected into the right flank of each mouse. The primary tumor was eliminated by surgery or PTT at day 0 and the sizes of distant tumors were measured.

Immunoassay in distant tumors

To analyze the immune cells in secondary tumors, those tumors were collected from mice in different groups, homogenized into single-cell

suspensions, and stained with anti–CD3-FITC (BioLegend, clone: 145-2C11, catalog no. 100306, lot: B241616), anti–CD4-PE (Invitrogen, clone: GK1.5, lot: 4326378), and anti–CD8-APC (BioLegend, clone: 53-6.7, catalog no. 100712, lot: B266721) antibodies according to the manufacturer's protocols. CTLs were $CD3^+CD4^-CD8^+$. To analyze $CD4^+$ helper T cells, those cells were further stained with anti–Foxp3-PE (eBioscience, clone: NRRF-30, catalog no. 12-4771) and anti–CD4-PerCP (BioLegend, clone: GK1.5, catalog no. 100432) according to the standard protocols. $CD4^+$ helper T cells could be classified into T_{regs} ($CD4^+Foxp3^+$) and effector T cells ($CD4^+Foxp3^-$). Also, TNF-α (Dakewe Biotech) and IFN-γ (Dakewe Biotech) in the serum in each group were analyzed with ELISA kits according to the manufacturer's protocols.

Orthotopic murine breast cancer model

To prepare 4T1 orthotopic murine breast cancer model, fLuc-4T1 cells (1×10^5) were inoculated into the breast pad of each mouse. Ten days later, the primary tumor on each mouse was removed by surgery or PTT. Afterward, mice were imaged by an IVIS (Interactive Video Information System) in vivo animal imaging system to observe the spontaneous metastasis. For the combination with ICB therapy, mice in certain groups were intravenously injected with 20 μg of anti–CTLA-4 on days 14, 17, and 20.

Immune memory assessment

After the elimination of primary CT26 tumors by surgery or bacteria plus laser for 40 days, the second batch of CT26 cells (1×10^6) was subcutaneously injected into those mice again. The tumor sizes were then closely recorded. For analyzing the percent of memory T cells, spleens harvested from mice in different groups were stained with anti–CD3-FITC (BioLegend, clone: 145-2C11, catalog no. 100306, lot: B241616), anti–CD8-PerCP-Cy5.5 (eBioscience, clone: 53-6.7, catalog no. E08300-1633), anti–CD62L-APC (eBioscience, clone: MEL-14, lot: 4300018), and anti–CD44-PE (BioLegend, clone: IM7, catalog no. 103007, lot: B185651) antibodies according to the manufacturers' protocols. Flow cytometry was used for analyzing the percentage of T_{CM} ($CD3^+CD8^+CD62L^+CD44^+$) and T_{EM} ($CD3^+CD8^+CD62L^-CD44^+$).

Statistical analysis

Statistical significance of the treatment groups was evaluated using Student's *t* test or one-way analysis of variance (ANOVA) with the least significant difference post hoc test. $^*P < 0.05$, $^{**}P < 0.01$, and $^{***}P < 0.001$ were considered statistically significant in analyses. Statistical details of the experiments were included in the figure captions.

SUPPLEMENTARY MATERIALS

Supplementary material for this article is available at http://advances.sciencemag.org/cgi/content/full/6/33/eaba3546/DC1

View/request a protocol for this paper from *Bio-protocol*.

REFERENCES AND NOTES

1. J. D. Raman, Urothelial cancer: Optimizing and integrating cisplatin-based chemotherapy across the disease spectrum. *Nat. Rev. Urol.* **15**, 139–140 (2018).
2. Y. Yamaoka, How to eliminate gastric cancer-related death worldwide? *Nat. Rev. Clin. Oncol.* **15**, 407–408 (2018).
3. D. E. J. G. J. Dolmans, D. Fukumuar, R. K. Jain, Photodynamic therapy for cancer. *Nat. Rev. Cancer* **3**, 380–387 (2003).
4. A. R. Rastinehad, H. Anastos, E. Wajswol, J. S. Winoker, J. P. Sfakianos, S. K. Doppalapudi, M. R. Carrick, C. J. Knauer, B. Taouli, S. C. Lewis, A. K. Tewari, J. A. Schwartz, S. E. Canfield, A. K. George, J. L. West, N. J. Halas, Gold nanoshell-localized photothermal ablation of prostate tumors in a clinical pilot device study. *Proc. Natl. Acad. Sci. U.S.A.* **116**, 18590–18596 (2019).
5. W. Zou, Regulatory T cells, tumour immunity and immunotherapy. *Nat. Rev. Immunol.* **6**, 295–307 (2006).
6. S. A. Patel, A. J. Minn, Combination cancer therapy with immune checkpoint blockade: Mechanisms and strategies. *Immunity* **48**, 417–433 (2018).
7. R. W. Jenkins, D. A. Barbie, K. T. Flaherty, Mechanisms of resistance to immune checkpoint inhibitors. *Br. J. Cancer* **118**, 9–16 (2018).
8. X. Zhao, S. Subramanian, Intrinsic resistance of solid tumors to immune checkpoint blockade therapy. *Cancer Res.* **77**, 817–822 (2017).
9. Q. Chen, J. Chen, Z. Yang, J. Xu, L. Xu, C. Liang, X. Han, Z. Liu, Nanoparticle-enhanced radiotherapy to trigger robust cancer immunotherapy. *Adv. Mater.* **31**, e1802228 (2019).
10. R. Kuai, W. Yuan, S. Son, J. Nam, Y. Xu, Y. Fan, A. Schwendeman, Elimination of established tumors with nanodisc-based combination chemoimmunotherapy. *Sci. Adv.* **4**, eaao1736 (2018).
11. Q. Chen, L. Xu, C. Liang, C. Wang, R. Peng, Z. Liu, Photothermal therapy with immune-adjuvant nanoparticles together with checkpoint blockade for effective cancer immunotherapy. *Nat. Commun.* **7**, 13193 (2016).
12. D. L. Lamm, B. A. Blumenstein, E. D. Crawford, J. E. Montie, P. Scardino, H. B. Grossman, T. H. Stanisic, J. A. Smith, J. Sullivan, M. F. Sarosdy, J. D. Crissman, C. A. Coltman, A randomized trial of intravesical doxorubicin and immunotherapy with bacille Calmette–Guérin for transitional-cell carcinoma of the bladder. *N. Engl. J. Med.* **325**, 1205–1209 (1991).
13. D. Romero, Immunotherapy: Oncolytic viruses prime antitumour immunity. *Nat. Rev. Clin. Oncol.* **15**, 135 (2018).
14. O. Felfoul, M. Mohammadi, S. Taherkhani, D. de Lanauze, Y. Zhong Xu, D. Loghin, S. Essa, S. Jancik, D. Houle, M. Lafleur, L. Gaboury, M. Tabrizian, N. Kaou, M. Atkin, T. Vuong, G. Batist, N. Beauchemin, D. Radzioch, S. Martel, Magneto-aerotactic bacteria deliver drug-containing nanoliposomes to tumour hypoxic regions. *Nat. Nanotechnol.* **11**, 941–947 (2016).
15. W. Quispe-Tintaya, D. Chandra, A. Jahangir, M. Harris, A. Casadevall, E. Dadachova, C. Gravekamp, Nontoxic radioactive *Listeria*^{at} is a highly effective therapy against metastatic pancreatic cancer. *Proc. Natl. Acad. Sci. U.S.A.* **110**, 8668–8673 (2013).
16. S. Zhou, C. Gravekamp, D. Bermudes, K. Liu, Tumour-targeting bacteria engineered to fight cancer. *Nat. Rev. Cancer* **18**, 727–743 (2018).
17. S. Leschner, K. Westphal, N. Dietrich, N. Viegas, J. Jablonska, M. Lyszkiewicz, S. Lienenklaus, W. Falk, N. Gekara, H. Loessner, S. Weiss, Tumor invasion of *Salmonella enterica* serovar Typhimurium is accompanied by strong hemorrhage promoted by TNF-α. *PLOS ONE* **4**, e6692 (2009).
18. F. Avogadri, C. Martinoli, L. Petrovska, C. Chiodoni, P. Transidico, V. Bronte, R. Longhi, M. Colombo, G. Dougan, M. Rescigno, Cancer immunotherapy based on killing of *Salmonella*-infected tumor cells. *Cancer Res.* **65**, 3920–3927 (2005).
19. N. Iida, A. Dzutsev, C. A. Stewart, L. Smith, N. Bouladoux, R. A. Weingarten, D. A. Molina, R. Salcedo, T. Back, S. Cramer, R.-M. Dai, H. Kiu, M. Cardone, S. Naik, A. K. Patri, E. Wang, F. M. Marincola, K. M. Frank, Y. Belkaid, G. Trinchieri, R. S. Goldszmid, Commensal bacteria control cancer response to therapy by modulating the tumor microenvironment. *Science* **342**, 967–970 (2013).
20. K. Low, M. Ittensohn, T. Le, J. Platt, S. Sodi, M. Amoss, O. Ash, E. Carmichael, A. Chakraborty, J. Fischer, S. L. Lin, X. Luo, S. I. Miller, L. Zheng, I. King, J. M. Pawelek, D. Bermudes, Lipid A mutant *Salmonella* with suppressed virulence and TNFα induction retain tumor-targeting in vivo. *Nat. Biotechnol.* **17**, 37–41 (1999).
21. H. S. Na, H. J. Kim, H.-C. Lee, Y. Hong, J. H. Rhee, H. E. Choy, Immune response induced by *Salmonella typhimurium* defective in ppGpp synthesis. *Vaccine* **24**, 2027–2034 (2006).
22. J.-H. Jeong, M. Song, S.-I. Park, K.-O. Cho, J. H. Rhee, H. E. Choy, *Salmonella enterica* serovar Gallinarum requires ppGpp for internalization and survival in animal cells. *J. Bacteriol.* **190**, 6340–6350 (2008).
23. J. F. Toso, V. J. Gill, H. Patrick, F. M. Marincola, N. P. Restifo, D. J. Schwartzentruber, R. M. Sherry, S. L. Topalian, J. C. Yang, F. Stock, L. J. Freezer, K. E. Morton, C. Seipp, L. Haworth, S. Mavroukakis, D. White, S. MacDonald, J. Mao, M. Sznol, S. A. Rosenberg, Phase I study of the intravenous administration of attenuated *Salmonella typhimurium* to patients with metastatic melanoma. *J. Clin. Oncol.* **20**, 142–152 (2002).
24. D. M. Heimann, S. A. Rosenberg, Continuous intravenous administration of live genetically modified *Salmonella typhimurium* in patients with metastatic melanoma. *J. Immunother.* **26**, 179–180 (2015).
25. J. H. Zheng, V. H. Nguyen, S.-N. Jiang, S.-H. Park, W. Tan, S. H. Hong, M. G. Shin, I.-J. Chung, Y. Hong, H.-S. Bom, H. E. Choy, S. E. Lee, J. H. Rhee, J.-J. Min, Two-step enhanced cancer immunotherapy with engineered *Salmonella typhimurium* secreting heterologous flagellin. *Sci. Transl. Med.* **9**, eaak9537 (2017).

26. S. Taherkhani, M. Mohammadi, J. Daoud, S. Martel, M. Tabrizian, Covalent binding of nanoliposomes to the surface of magnetotactic bacteria for the synthesis of self-propelled therapeutic agents. *ACS Nano* **8**, 5049–5060 (2014).
27. M.-H. Xiong, Y. Bao, X.-J. Du, Z.-B. Tan, Q. Jiang, H.-X. Wang, Y.-H. Zhu, J. Wang, Differential anticancer drug delivery with a nanogel sensitive to bacteria-accumulated tumor artificial environment. *ACS Nano* **7**, 10636–10645 (2013).
28. W. Chen, Y. Wang, M. Qin, X. Zhang, Z. Zhang, X. Sun, Z. Gu, Bacteria-driven hypoxia targeting for combined biotherapy and photothermal therapy. *ACS Nano* **12**, 5995–6005 (2018).
29. C.-H. Luo, C.-T. Huang, C.-H. Su, C.-S. Yeh, Bacteria-mediated hypoxia-specific delivery of nanoparticles for tumors imaging and therapy. *Nano Lett.* **16**, 3493–3499 (2016).
30. N. Agrawal, C. Bettegowda, I. Cheong, J.-F. Geschwind, C. G. Drake, E. L. Hipkiss, M. Tatsumi, L. H. Dang, L. A. Diaz Jr., M. Pomper, M. Abusedera, R. L. Wahl, K. W. Kinzler, S. Zhou, D. L. Huso, B. Vogelstein, Bacteriolytic therapy can generate a potent immune response against experimental tumors. *Proc. Natl. Acad. Sci. U.S.A.* **101**, 15172–15177 (2004).
31. C. Clairmont, K. C. Lee, J. Pike, M. Ittensohn, K. B. Low, J. Pawelek, D. Bermudes, S. M. Brecher, D. Margitich, J. Turnier, Z. Li, X. Luo, I. King, L. M. Zheng, Biodistribution and genetic stability of the novel antitumor agent VNP20009, a genetically modified strain of *Salmonella typhimurium*. *J. Infect. Dis.* **181**, 1996–2002 (2000).
32. Y. A. Yu, T. M. Shabahang STimiryasova, Q. Zhang, R. Beltz, I. Gentschev, W. Goebel, A. A. Szalay, Visualization of tumors and metastases in live animals with bacteria and vaccinia virus encoding light-emitting proteins. *Nat. Biotechnol.* **22**, 313–320 (2004).
33. A. C. Montezano, K. B. Neves, R. A. Lopes, F. Rios, Isolation and culture of endothelial cells from large vessels. *Hypertension* **15**, 345–348 (2017).
34. B. C. Baguley, Antivascular therapy of cancer: DMXAA. *Lancet Oncol.* **4**, 141–148 (2003).
35. F. Saccheri, C. Pozzi, F. Avogadri, S. Barozzi, M. Faretta, P. Fusi, M. Rescigno, Bacteria-induced gap junctions in tumors favor antigen cross-presentation and antitumor immunity. *Sci. Transl. Med.* **2**, 44ra57 (2010).
36. V. Gopalakrishnan, C. N. Spencer, L. Nezi, A. Reuben, M. C. Andrews, T. V. Karpinets, P. A. Prieto, D. Vicente, K. Hoffman, S. C. Wei, A. P. Cogdill, L. Zhao, C. W. Hudgens, D. S. Hutchinson, T. Manzo, M. P. de Macedo, T. Cotechini, T. Kumar, W. S. Chen, S. M. Reddy, R. S. Sloane, J. Galloway-Pena, H. Jiang, P. L. Chen, E. J. Shpall, K. Rezvani, A. M. Alousi, R. F. Chemaly, S. Shelburne, L. M. Vence, P. C. Okhuysen, V. B. Jensen, A. G. Swennes, F. McAllister, E. M. R. Sanchez, Y. Zhang, E. Le Chatelier, L. Zitvogel, N. Pons, J. L. Austin-Breneman, L. E. Haydu, E. M. Burton, J. M. Gardner, E. Sirmans, J. Hu, A. J. Lazar, T. Tsujikawa, A. Diab, H. Tawbi, I. C. Glitza, W. J. Hwu, S. P. Patel, S. E. Woodman, R. N. Amaria, M. A. Davies, J. E. Gershenwald, P. Hwu, J. E. Lee, J. Zhang, L. M. Coussens, Z. A. Cooper, P. A. Futreal, C. R. Daniel, N. J. Ajami, J. F. Petrosino, M. T. Tetzlaff, P. Sharma, J. P. Allison, R. R. Jenq, J. A. Wargo, Gut microbiome modulates response to anti–PD-1 immunotherapy in melanoma patients. *Science* **359**, 97–103 (2018).
37. M. Vétizou, J. M. Pitt, R. Daillére, P. Lepage, N. Waldschmitt, C. Flament, S. Rusakiewicz, B. Routy, M. P. Roberti, C. P. M. Duong, V. Poirier-Colame, A. Roux, S. Becharef, S. Formenti, E. Golden, S. Cording, G. Eberl, A. Schlitzer, F. Ginhoux, S. Mani, T. Yamazaki, N. Jacquelot, D. P. Enot, M. Bérard, J. Nigou, P. Opolon, A. Eggermont, P.-L. Woerther, E. Chachaty, N. Chaput, C. Robert, C. Mateus, G. Kroemer, D. Raoult, I. G. Boneca, F. Carbonnel, M. Chamaillard, L. Zitvogel, Anticancer immunotherapy by CTLA-4 blockade relies on the gut microbiota. *Science* **350**, 1079–1084 (2015).
38. C. T. Nguyen, S. H. Hong, J.-I. Sin, V. D. V. Hong, K. Jeong, K. O. Cho, S. Uematsu, S. Akira, S. E. Lee, J. H. Rhee, Flagellin enhances tumor-specific $CD8^+$ T cell immune responses through TLR5 stimulation in a therapeutic cancer vaccine model. *Vaccine* **31**, 3879–3887 (2013).
39. L. Sfondrini, A. Rossini, D. Besusso, A. Merlo, E. Tagliabue, S. Mènard, A. Balsari, Antitumor activity of the TLR-5 ligand flagellin in mouse models of cancer. *J. Immunol.* **176**, 6624–6630 (2006).
40. S. M. Kaech, E. J. Wherry, R. Ahmed, Effector and memory T-cell differentiation: Implications for vaccine development. *Nat. Rev. Immunol.* **2**, 251–262 (2002).

Acknowledgments: We thank P. Rong in the Third Xiangya Hospital of Central South University for providing the ΔppGpp *S. typhimurium*. **Funding:** This work was partially supported by the National Key Research Programs of China (2016YFA0201200), the National Natural Science Foundation of China (31822022, U1932208, 51525203, 51761145041, and 21927803), a Jiangsu Natural Science Fund for Outstanding Youth Science Foundation (BK20180094), and the Collaborative Innovation Center of Suzhou Nano Science and Technology. **Author contributions:** K.Y. and Z.L. conceived the project; X.Y. and H.Z. carried out bacteria experiments; X.Y., H.Z., and S.X. carried out PA imaging and PTT of tumor; X.Y., Y.C., and J.Z. carried out the immunological experiment. K.Y., Z.L., and X.Y. provided guidance on experimental design and wrote the manuscript. Z.C. reviewed the manuscript. **Competing interests statement:** The authors declare that they have no competing interests. **Data and materials availability:** All data needed to evaluate the conclusions in the paper are present in the paper and/or the Supplementary Materials. Additional data related to this paper may be requested from the authors. Correspondence and requests for materials should be addressed to the corresponding authors K.Y. (kyang@suda.edu.cn) and Z.L. (zliu@suda.edu.cn).

Submitted 26 November 2019
Accepted 2 July 2020
Published 14 August 2020
10.1126/sciadv.aba3546

Citation: X. Yi, H. Zhou, Y. Chao, S. Xiong, J. Zhong, Z. Chai, K. Yang, Z. Liu, Bacteria-triggered tumor-specific thrombosis to enable potent photothermal immunotherapy of cancer. *Sci. Adv.* **6**, eaba3546 (2020).